# A geometrically nonlinear floating node method for damage modelling of composites

Zhi, J.; Chen, B. Y.; Tay, T. E.

**Publication date**
2020

**Document Version**
Final published version

**Published in**
ECCM 2018 - 18th European Conference on Composite Materials

# A GEOMETRICALLY NONLINEAR FLOATING NODE METHOD FOR DAMAGE MODELLING OF COMPOSITES

J. Zhi[1], B.Y. Chen[2], T.E. Tay[1]

[1] Department of Mechanical Engineering, National University of Singapore
9 Engineering Drive 1, 117575, Singapore
Email: mpetayte@nus.edu.sg and Jie.zhi@u.nus.edu
Webpage: http://www.me.nus.edu.sg
[2] Faculty of Aerospace Engineering, Delft University of Technology
2629 HS Delft, Netherlands
Email: B.Chen-2@tudelft.nl
Webpage: https://www.tudelft.nl/?id=3842

**Keywords:** Discrete crack methods, large displacement, matrix cracking, delamination

**Abstract**
Tremendous efforts have been put into the study of structural integrity and the understanding of failure mechanisms in composites. Geometric non-linearity, receiving few attention in coupon-level simulations, can play an important role in the design and analysis of larger structures. This paper aims at extending the recently-developed *Floating Node Method* for damage analysis of laminated composites subjected to large deformations. The kinematics of strong discontinuities including interfacial delamination and matrix cracks are explicitly described in a geometrically nonlinear framework. Interactions between these two kinds of failure patterns are enabled through enriched elements equipped with floating nodes. To verify this proposed method, buckling-induced delamination and low-velocity impact damage are modelled, the results of which show good agreement with results from literature.

## 1. Introduction

Damage modelling and failure prediction are essential for the application of composites. They have been extensively studied with *continuum damage methods*, in which the effect of diffuse cracks is smeared out over the continuum. Recently, high-fidelity simulation has been achieved with *discrete crack methods*, and physical cracks such as matrix cracking and delamination can be captured explicitly by including crack kinematics in finite element formulations [1-3].

Chen et al. proposed *Floating Node Method* (FNM) for modelling multiple discontinuities in a finite element, which can also capture the interaction between matrix cracking and delamination [3]. This method has been further developed for the simulation of tensile failure and delamination migration [4, 5]. In this work, a 2D geometrically nonlinear formulation of the FNM is presented for modelling damage growth in composites undergoing large displacements. Enriched solid elements and cohesive elements are developed with consideration of the displacement jump in the deformation map and discontinuities in other kinematics. The matrix cracks within 90-degree plies and interfacial delamination between plies are simulated with a mixed-mode cohesive model. The proposed formulation are verified with two numerical examples involving buckling-induced delamination and low-velocity impact, respectively.

## 2. FE formulation of strong discontinuities in matrix cracking and delamination

### 2.1. Governing equations

Considering a solid $\Omega$ with displacement boundary $\partial_u\Omega$, traction boundary $\partial_t\Omega$ and cohesive cracks $\Gamma$, the governing equations can be expressed with respect to the reference configuration:

$$\begin{aligned} \mathrm{DIV}\,\boldsymbol{P} + \rho_0\boldsymbol{B} &= \rho_0\ddot{\boldsymbol{u}} \quad \text{in } \Omega_0/\Gamma_0 \\ \boldsymbol{u} &= \hat{\boldsymbol{u}} \quad \text{on } \partial_u\Omega_0 \\ \boldsymbol{P}\cdot\boldsymbol{N} &= \hat{\boldsymbol{T}} \quad \text{on } \partial_t\Omega_0 \\ \boldsymbol{P}\cdot\boldsymbol{N}^- &= -\boldsymbol{P}\cdot\boldsymbol{N}^+ = \boldsymbol{T}_c \quad \text{on } \Gamma_0 \end{aligned} \tag{1}$$

where $\boldsymbol{P}$ is the first *Piola-Kirchhoff* stress, $\boldsymbol{B}$ is the body force and $\boldsymbol{T}_c$ is the cohesive traction. The weak formulation of Eq. (1) is given as:

$$\int_{\Omega_0/\Gamma_0} \boldsymbol{P}:\mathrm{Grad}\,\delta\boldsymbol{u}dV + \int_{\Gamma_0} \boldsymbol{T}_c\cdot[\![\delta\boldsymbol{u}]\!]dA = \int_{\Omega_0/\Gamma_0} \rho_0(\boldsymbol{B}-\ddot{\boldsymbol{u}})\cdot\delta\boldsymbol{u}dV + \int_{\partial_t\Omega_0} \hat{\boldsymbol{T}}\cdot\delta\boldsymbol{u}dA \tag{2}$$

The second *Piola-Kirchhoff* stress $\boldsymbol{S}$ is introduced and Eq. (2) can be reformulated as:

$$\delta\mathcal{W} = \delta\mathcal{W}_{\mathrm{kin}} + \delta\mathcal{W}_{\mathrm{int}} + \delta\mathcal{W}_{\mathrm{coh}} - \delta\mathcal{W}_{\mathrm{ext}} = 0 \tag{3}$$

where

$$\begin{aligned} \delta\mathcal{W}_{\mathrm{kin}} &= \int_{\Omega_0/\Gamma_0} \rho_0\ddot{\boldsymbol{u}}\cdot\delta\boldsymbol{u}dV \\ \delta\mathcal{W}_{\mathrm{int}} &= \int_{\Omega_0/\Gamma_0} \boldsymbol{S}:\delta\boldsymbol{E}dV \\ \delta\mathcal{W}_{\mathrm{coh}} &= \int_{\Gamma_0} \boldsymbol{T}_c\cdot[\![\delta\boldsymbol{u}]\!]dA = \int_{\Gamma} \boldsymbol{t}_c\cdot[\![\delta\boldsymbol{u}]\!]da \\ \delta\mathcal{W}_{\mathrm{ext}} &= \int_{\Omega_0/\Gamma_0} \rho_0\boldsymbol{B}\cdot\delta\boldsymbol{u}dV + \int_{\partial_t\Omega_0} \hat{\boldsymbol{T}}\cdot\delta\boldsymbol{u}dA \end{aligned} \tag{4}$$

The constitutive equations include the elastic orthotropic behavior for bulk layers and cohesive behavior for matrix cracks and interface cracks. *Rankine* criterion is adopted to evaluate the fracture of the bulk element and also the crack direction $\boldsymbol{n}$.

### 2.2. Enriched solid elements and enriched interface elements

The domain $\Omega_0$ is discretized by $n_{el\_s}$ solid elements and $n_{el\_c}$ cohesive elements. Discretization of the weak formulation is given as:

$$\boldsymbol{\delta d}^T\boldsymbol{R} = 0 \rightarrow \boldsymbol{R} = \mathcal{A}(\boldsymbol{R}_s, \boldsymbol{R}_c) = 0 \tag{5}$$

where $\boldsymbol{d}$ denotes nodal displacement and $\boldsymbol{R}_s$, $\boldsymbol{R}_c$ are residuals related to solid elements and cohesive elements, which are written as:

$$\boldsymbol{R}_s = \mathcal{A}_{e=1}^{n_{el\_s}}\left(\int_{\Omega_0^e}\rho_0\boldsymbol{N}^{eT}\boldsymbol{N}^e dV\ddot{\boldsymbol{d}}^e + \int_{\Omega_0^e}\boldsymbol{B}_L^{eT}\{\boldsymbol{S}\}dV - \int_{\partial_t\Omega_0^e}\boldsymbol{N}^{eT}\hat{\boldsymbol{T}}dV\right) \tag{6}$$

and

$$\boldsymbol{R}_c = \mathcal{A}_{e=1}^{n_{el\_c}} \left( \int_{\Gamma^e} \boldsymbol{L}^{eT} \boldsymbol{t}_c dV \right) \tag{7}$$

where $\boldsymbol{N}^e$, $\boldsymbol{B}_L^e$ and $\boldsymbol{L}^e$ are finite element matrices.

Once *Rankine* criterion is satisfied, the crack direction determines the location of floating nodes and the solid element is partitioned into several sub-elements, one scenario of which is shown in Fig. 1 (a). The residual of this enriched solid element can be given as the assembly of sub-elements:

$$\boldsymbol{R}_{ers}^e = \mathcal{A} \left( \boldsymbol{R}_s^e|_{\Omega_0^{e(1)}}, \boldsymbol{R}_s^e|_{\Omega_0^{e(2)}}, \boldsymbol{R}_c^e|_{\Gamma^e} \right) \tag{8}$$

When crack reaches the edge of an interface element as illustrated in Fig. 1 (b), the interface element is also partitioned in a similar manner to ensure that the interaction between intra-ply crack and inter-ply crack is accurately captured. The residual is expressed as:

$$\boldsymbol{R}_{erc}^e = \mathcal{A} \left( \boldsymbol{R}_c^e|_{\bar{\Gamma}^{e(1)}}, \boldsymbol{R}_c^e|_{\bar{\Gamma}^{e(2)}} \right) \tag{9}$$

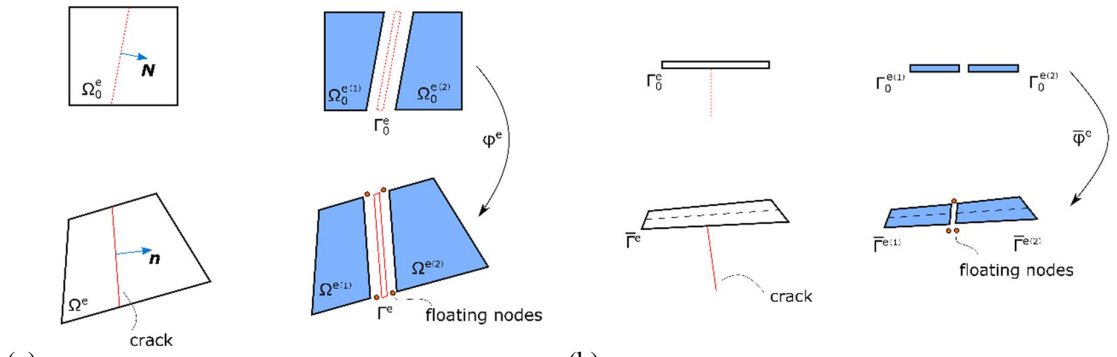


**Figure 1.** (a) Enriched solid elements; (b) Enriched cohesive elements.

## 3. Numerical implementation

A compact form of FE equations can be written as:

$$\boldsymbol{M}\ddot{\boldsymbol{d}} + \boldsymbol{F}_{\text{int}}(\boldsymbol{d}) + \boldsymbol{F}_{\text{coh}}(\boldsymbol{d}) - \boldsymbol{F}_{\text{ext}} = 0 \tag{10}$$

where $\boldsymbol{d}$ is nodal displacement, $\boldsymbol{M}$ is the global mass matrix and $\boldsymbol{F}$ is global force vector ("int": internal force in solid elements; "coh": internal force in cohesive elements; "ext": external force). Implicit time integration with a *Hilber-Hughes-Taylor* (HHT) operator is adopted to solve this dynamic problem. The equation to be solved at step $t_{n+1}$ is given as:

$$\begin{aligned} \boldsymbol{R}(\boldsymbol{d}_{n+1}) = \boldsymbol{M}\ddot{\boldsymbol{d}}_{n+1} + (1+\alpha)\left[\boldsymbol{F}_{\text{int}}(\boldsymbol{d}_{n+1}) + \boldsymbol{F}_{\text{coh}}(\boldsymbol{d}_{n+1}) - \boldsymbol{F}_{\text{ext},n+1}\right] \\ -\alpha\left[\boldsymbol{F}_{\text{int}}(\boldsymbol{d}_n) + \boldsymbol{F}_{\text{coh}}(\boldsymbol{d}_n) - \boldsymbol{F}_{\text{ext},n}\right] = 0 \end{aligned} \tag{11}$$

Substitute the expression of $\ddot{\boldsymbol{d}}_{n+1}$ by the Newmark formula, Eq. (11) can be written with $\boldsymbol{d}_{n+1}$ as the only unknown variable and the linearization of the residual in Eq. (11) is computed as:

$$\boldsymbol{R}\left(\boldsymbol{d}_{n+1}^{(k)}\right) + \left.\frac{\partial \boldsymbol{R}}{\partial \boldsymbol{d}}\right|_{\boldsymbol{d}_{n+1}^{(k)}} \Delta \boldsymbol{d}_{n+1}^{(k)} = 0 \tag{12}$$

where $k$ is the iteration number and the tangent stiffness matrix is given as:

$$\frac{\partial \boldsymbol{R}}{\partial \boldsymbol{d}} = \frac{\boldsymbol{M}}{\beta \Delta t^2} + (1+\alpha)\left(\frac{\partial \boldsymbol{F}_{\text{int}}}{\partial \boldsymbol{d}} + \frac{\partial \boldsymbol{F}_{\text{coh}}}{\partial \boldsymbol{d}}\right) \tag{13}$$

where $\alpha$ and $\beta$ are numerical parameters used in the HHT method. The displacements can be updated as $\boldsymbol{d}_{n+1}^{(k+1)} = \boldsymbol{d}_{n+1}^{(k)} + \Delta \boldsymbol{d}_{n+1}^{(k)}$. Inertial term can be ignored if a quasi-static problem is solved.

## 4. Numerical examples

### 4.1. Buckling-induced delamination

The first problem studied is buckling-induced delamination posed in [6], as illustrated in Fig. 2. Two composite beams with predefined cracks are loaded by a horizontal rightward displacement $u$. Buckling is triggered by a small displacement $u_0$, which introduces an initial imperfection for post-buckling analysis. Subsequently, mode-I delamination propagates along the interface with the opening of the two arms of the buckled beam. Geometric parameters and material properties are listed in Table 1.

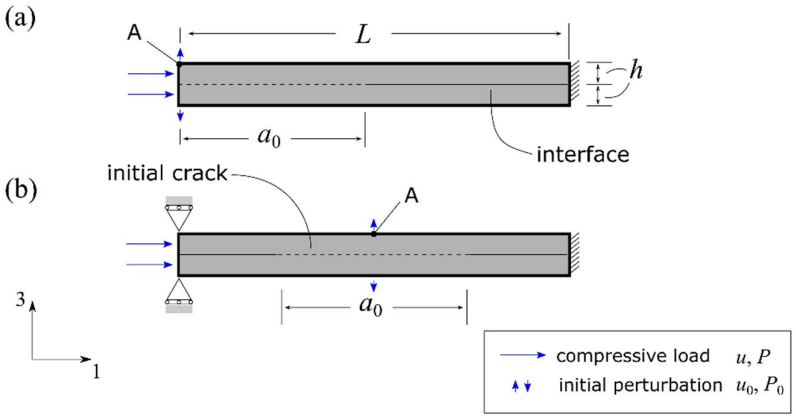


**Figure 2.** Composite beam with initial cracks (a) case-1, (b) case-2.

**Table 1.** Geometric parameters and material properties [6].

| Geometric parameters | | Material properties | |
|---|---|---|---|
| $L$ (mm) | 20 | $E_1$ (GPa) | 135 |
| $2h$ (mm) | 0.4 | $G_{13}$ (GPa) | 5.7 |
| $w$ (mm) | 1 | $t_n^0$ (MPa) | 50 |
| $a_0$ (mm) | 10 | $G_{IC}$ (KJ/m$^2$) | 0.4 |
| - | - | $K$ (N/mm$^3$) | $10^6$ |

The beam is modelled with enriched solid elements and cohesive elements for 0-degree ply and interface, respectively. A mesh size of 0.05 mm is chosen and displacement control is used during simulation. The initial perturbation displacement is $6\times10^{-4}$ mm. Afterwards, a horizontal displacement is imposed and reaction force $P$ can be evaluated. For case-1, four fracture energy values ($G_{IC}$=0.2, 0.4, 0.8, 1.6 N/mm) are studied. The load-displacement curves are plotted in Fig. 3 (a) and compared with results given in [6]. As shown in Fig. 3 (a), the load $P$ increases a lot initially while the deflection at point 'A' remains small. With the onset of buckling, deflection starts increasing but the force remains the same. Finally, the delamination propagation causes the load drop. The result of case-2 in Fig. 3 (b) is similar but the peak load is larger and the deflection is smaller, as shown in Fig. 3 (c) and (d).

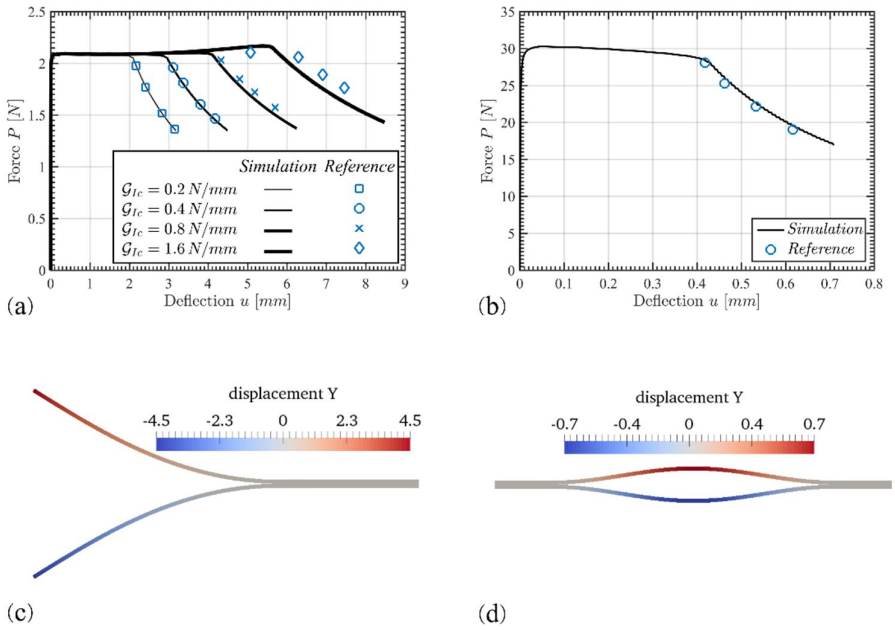


**Figure 3.** Response curves (a) case-1, (b) case-2; Deformation configurations (c) case-1, (d) case-2.

### 4.2. Low-velocity impact damage

In the second example, a carbon fiber reinforced composite beam is impacted by a cylindrical head [7] and the experimental setup is given in Fig. 4. The ply sequence of the laminate is $[0_5/90_3]_s$. The size of the beam is 100 mm×17 mm×4.8 mm and the diameter of the impacter is 40 mm. The impact analysis is simplified as a two-dimensional case, as shown in Fig. 4 (b). A half FE model is adopted considering symmetric boundary conditions. The impactor is discretized with 2D rigid elements and the mass for this half model is 392.5 g. Each ply is modelled with a single enriched solid element through the thickness and two interfaces are modelled with enriched cohesive elements. 0.25 mm mesh size is used along the length of the beam. Contact pairs are defined between the beam and the impactor, on which an initial downward velocity $v_0$=4.43 m/s is imposed.

**Table 2.** Material properties used in the simulations.

| Solid element | | Cohesive element | |
|---|---|---|---|
| $E_{11}$ (GPa) | 135 | $K$ (N/mm$^3$) | $10^6$ |
| $E_{22}$=$E_{22}$ (GPa) | 9.2 | $t_n^0$=$t_t^0$ (MPa) | 105 |
| $G_{12}$=$G_{13}$ (GPa) | 5.5 | $S_L$ (MPa) | 80 |
| $G_{23}$ (GPa) | 4.5 | $G_{IC}$ (KJ/m$^2$) | 0.26 |
| $\nu_{12}$=$\nu_{13}$ | 0.30 | $G_{IIC}$= $G_{IIIC}$ (KJ/m$^2$) | 0.84 |
| $\nu_{23}$ | 0.45 | - | - |
| $\rho$ (kg/m$^3$) | 1780 | - | - |
| $f_n$ (MPa) | 60 | - | - |

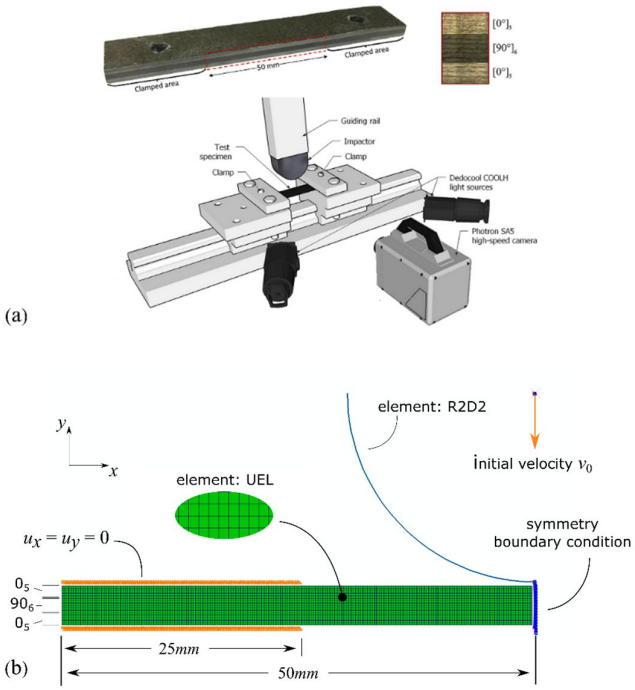


**Figure 4.** (a) Experimental setup [7]; (b) Numerical model.

The force-displacement curve is given in Fig. 5 (a). Periodic oscillations firstly occur during the initial elastic loading. When the curve reaches the point 'A', several diagonal matrix cracks initiate in the 90-degree plies as both shown in the experiment and simulation results in Fig. 5 (b). As caused by transverse shear stress, these cracks are usually denoted as "shear cracks". The location of these matrix cracks varies between 18.75-21.25 mm, close to experimental observations with an average distance 18.1 mm. The average angles between the crack and horizontal line in experiment and simulation are 49° and 45°, respectively. Shortly after the crack initiation, the load drops suddenly to almost zero at point 'B'. The lower interface crack propagates away from the center while the upper one propagates toward to the impact point and significant crack openings can be observed. After point 'B' in Fig. 5 (a), the contact force increases again, during which larger fluctuations can be observed as a result of the delamination and matrix cracks. When the residual kinetic energy of the impactor is consumed completely, the impactor starts rebounding and contact force decreases gradually.

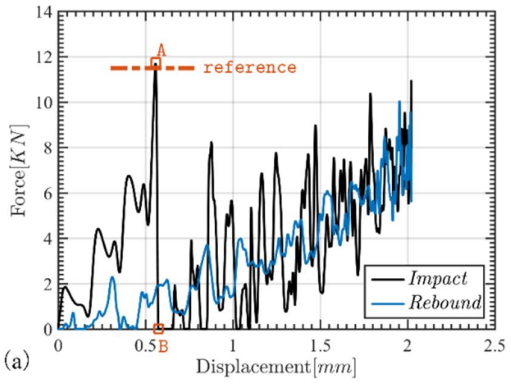

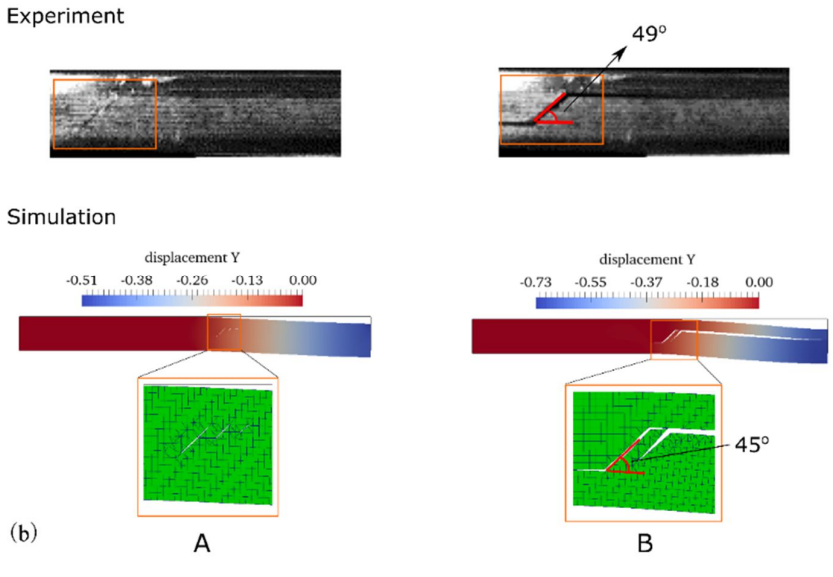


3

**Figure 5.** Results from simulation and experiment [7] (a) load-displacement curves, (b) failure patterns at point 'A' and 'B'.

## 5. Conclusions

In this presentation, the *Floating Node Method* for modelling matrix cracking and delamination in composite laminates in the large deformation range was developed. To verify the proposed method, two representative numerical examples were given. The first example shows a verification of the formulation in modelling buckling problems with geometric non-linearity. Buckling initiates, followed by delamination propagation due to transverse deformation. The second example examines the capability of this method in modelling coupled dynamic failure mechanisms in composites subjected to low-velocity impact. Diagonal matrix cracks are firstly observed. Delaminations along the upper and lower interfaces are then induced and propagate in opposite directions.

## References

[1] van der Meer FP, Sluys LJ. A phantom node formulation with mixed mode cohesive law for splitting in laminates. *Int J Fract*. 2009; 158: 107-24.

[2] Ling D, Yang Q, Cox B. An augmented finite element method for modeling arbitrary discontinuities in composite materials. *Int J Fract*. 2009; 156: 53-73.

[3] Chen BY, Pinho ST, De Carvalho NV, Baiz PM, Tay TE. A floating node method for the modelling of discontinuities in composites. *Eng Fract Mech*. 2014; 127: 104-34.

[4] Chen BY, Tay TE, Pinho ST, Tan VBC. Modelling the tensile failure of composites with the floating node method. *Comput Method Appl M*. 2016; 308: 414-42.

[5] Chen BY, Tay TE, Pinho ST, Tan VBC. Modelling delamination migration in angle-ply laminates. *Compos Sci Technol*. 2017; 142: 145-55.

[6] Allix O, Corigliano A. Geometrical and interfacial non-linearities in the analysis of delamination in composites. *Int J Solids Struct*. 1999; 36: 2189-216.

[7] Topac OT, Gozluklu B, Gurses E, Coker D. Experimental and computational study of the damage process in CFRP composite beams under low-velocity impact. *Compos Part A-Appl S*. 2017; 92: 167-82.